Acta Biomaterialia 191 (2025) 149–157

Contents lists available at ScienceDirect

Acta Biomaterialia

journal homepage: www.elsevier.com/locate/actbio

Full length article

Endochondral ossification: Insights into the cartilage mineralization processes achieved by an anhydrous freeze substitution protocol

Suwimon Boonrungsiman [a], Christopher Allen [b], Fabio Nudelman [c], Sandra Shefelbine [d], Colin Farquharson [e], Alexandra E Porter [f,*], Roland A Fleck [a,*]

[a] Centre for Ultrastructural Imaging (CUI), Kings College London, New Hunts House, Guys Hospital Campus, London SE1 1UL, UK
[b] Diamond Light Source Ltd, Diamond House, Harwell Science and Innovation Campus, Didcot, Oxfordshire OX11 0DE, UK
[c] School of Chemistry, University of Edinburgh, King's Buildings, Edinburgh EH9 3FJ, UK
[d] Department of Mechanical and Industrial Engineering and Department of Bioengineering, Northeastern University, Boston, MA, USA
[e] Roslin Institute and Royal (Dick) School of Veterinary Studies, University of Edinburgh, Easter Bush, Midlothian, EH25 9RG, UK
[f] Department of Materials, Imperial College London, London SW7 2AZ, UK

ARTICLE INFO

Keywords:
Biomineralization
Cartilage
Intracellular calcium phosphate
HPF-FS
Extracellular vesicles

ABSTRACT

Growth plate cartilage (GP) serves as a dynamic site of active mineralization and offers a unique opportunity to investigate the cell-regulated matrix mineralization process. Transmission electron microscopy (TEM) provides a means for the direct observation of these mechanisms, offering the necessary resolution and chemical analysis capabilities. However, as mineral crystallinity is prone to artifacts using aqueous fixation protocols, sample preparation techniques are critical to preserve the mineralized tissue in its native form. We optimized cryo-fixation by high-pressure freezing followed by freeze substitution in anhydrous acetone containing 0.5 % uranyl acetate to prepare murine GP for TEM analysis. This sample preparation workflow maintains cellular and extracellular protein structural integrity with sufficient contrast for observation and without compromising mineral crystallinity. By employing appropriate sample preparation techniques, we were able to observe two parallel mineralization processes driven by chondrocytes: 1) intracellular- and 2) extracellular-originating mineralized vesicles. Both mechanisms are based on sequestering calcium phosphate (CaP) within a membrane-limited structure, *albeit* originating from different compartments of the chondrocytes. In the intracellular originating pathway, CaP accumulates within mitochondria as globular CaP granules, which are incorporated into intracellular vesicles (500–1000 nm) and transported as granules to the extracellular matrix (ECM). In contrast, membrane budding vesicles with a size of approximately 100–200 nm, filled with needle-shaped minerals were observed only in the ECM. Both processes transport CaP to the collagenous matrix *via* vesicles, they can be differentiated based on the vesicle size and mineral morphologies. Their individual importance to the cartilage mineralization process is yet to be determined.

Statement of Significance: We do not fully understand the process by which epiphyseal cartilage mineralizes - a vital step in endochondral bone formation. Previous work has proposed that mitochondria and intracellular vesicles are storage sites for the delivery of mineral to collagen fibrils. However, these concepts are founded on results from *in vitro* models of mineralization; no prior work has observed mineral-containing intracellular vesicles or mitochondria in developing epiphyseal cartilage. Here we developed a new cryofixation preparation route for transmission electron microscopy (TEM) imaging that has disclosed a cell-regulated process of mineralization in epiphyseal cartilage. High resolution TEM images revealed an involvement of mitochondria and intracellular and extracellular vesicles in delivering transient mineral phases to the collagen fibrils to promote cartilage mineralization.

Abbreviations: TEM, transmission electron microscope; HPF, high-pressure freezing; FS, freeze substitution; CaP, calcium phosphate; ECM, extracellular matrix.

* Corresponding authors.
E-mail addresses: a.porter@imperial.ac.uk (A.E. Porter), roland.fleck@kcl.ac.uk (R.A. Fleck).

https://doi.org/10.1016/j.actbio.2024.11.015
Received 17 September 2024; Received in revised form 28 October 2024; Accepted 11 November 2024
Available online 12 November 2024

1. Introduction

Despite decades of research investigating long bone formation during development, we still do not fully understand the process by which epiphyseal cartilage mineralizes - a vital step in endochondral bone formation. This process is essential for the formation and linear growth of long bones, such as the tibia and femur, during which the epiphyseal cartilage template ossifies and is replaced by bone. In the epiphyseal growth plate (GP), chondrocytes undergo terminal differentiation and those within the hypertrophic zone secrete a collagen-type X-rich extracellular matrix (ECM) which is mineralized prior to its resorption by osteoclasts. The remaining cartilage remnants act as a scaffold for bone-forming osteoblasts which secrete a collagen type 1-rich osteoid that is mineralized over time [1,2].

Several different mechanisms have been proposed to explain how the calcium/phosphate (CaP) rich mineral is delivered to the collagen fibrils within the ECM. Electron microscopy has shown that in the ECM, osteoblasts and chondrocytes produce matrix vesicles (MV) that bud from the plasma membranes [3,4]. These MVs accumulate P and Ca ions and provide a microenvironment suitable for CaP mineral nucleation [4] which occurs through the activities of enzymes and proteins that are membrane-bound or reside within the MV lumen [4–7]. The isolated MVs are 100–300 nm in diameter and able to bind to the ECM via a number of collagen-binding proteins [8,9]. Studies have suggested that the first mineral formed in MVs is a highly transient amorphous calcium phosphate (ACP) [10], which is released from the MVs and deposited within the gap regions of collagen fibrils, where it transforms into crystalline needles or plates of CaP [11]. The infiltration of the ACP into the collagen has been proposed to be mediated by interactions between non-collagenous proteins and the gap regions in the fibrils. Once the amorphous phase is inside the collagen, it nucleates into hydroxyapatite [12,13]. A more recent and alternative hypothesis to explain collagen fibril mineralization involves the sequestration of CaP inside intracellular vesicles and mitochondria of both osteoblasts and chondrocytes [14–16]. Mitochondria are required for oxidative phosphorylation but they have many other functions, including the ability to take up and store calcium [17]. Transmission electron microscopy (TEM) of cultured osteoblasts has shown that mitochondria containing CaP granules fuse with neighboring vesicles, suggesting that they store CaP for subsequent transportation – *via* intra then extracellular vesicles - to the collagenous ECM [14,18]. However, these concepts are founded on results from *in vitro* models of mineralization [14], mineralization of zebrafish fin rays [15] and mouse parietal bone [16]. No prior work has observed mineral-containing intracellular vesicles, mitochondria or vesicles delivering ACP from inside the cells to the ECM to mineralise the collagen in developing *epiphyseal cartilage*. The identification of intracellular trafficking of mineral within the chondrocytes of the growth plate will enhance our understanding of cartilage matrix mineralisation and the endochondral ossification process. The form in which the mineral is delivered from the vesicles to the collagen fibrils remains unclear.

To enable the observation of these mineralization steps, sample preparation requires optimization to preserve both the mineral composition/crystallinity and cellular structure. In particular, the ACP phase will undergo a transformation into thermodynamically stable crystalline hydroxyapatite in a physiological solution [19]. This phenomenon has been documented when aqueous fixatives during sample preparation were used [20]. Conventional chemical fixation can also distort the ultrastructure of the cartilage matrix and create shrunken chondrocytes [2,21].

High-pressure freezing (HPF) followed by freeze substitution (FS), is the gold standard technique to preserve cartilage structure in its hydrated near-native state [22,23]. HPF omits the use of conventional chemical fixatives by rapidly freezing the sample under pressures of approximately 2000 bars [24,25]. Samples are fixed within a few milliseconds which is sufficient to capture short-lived biological events and structural preservation of the molecular structures within the tissues is improved [26]. After the HPF process, vitrified ice is replaced with solvents containing fixatives and staining agents, *i.e.* glutaraldehyde, osmium tetroxide, tannic acid, and uranyl acetate. This substitution process is performed at low temperatures, at which the fixatives are less active and molecular and ionic movements are significantly reduced [27–30]. 1–5 % water is normally added to the FS solution to improve membrane contrast. Walther and Ziegler [31], but the introduction of this small amount of water, either intentionally or unintentionally from fixative stocks, may change the crystallinity and structure of the mineral in the sample during several hours of the FS process [20].

Previous studies have focused on optimizing protocols for HPF-FS that preserve the mineralized ultrastructure but protocols to preserve, simultaneously, the mineral crystallinity, or distribution of Ca and P ions – a necessary requirement to characterize the mineralizing cartilage in its near-native state, have been neglected [32,33]. Therefore, the aim of this study was to develop a new and robust sample preparation workflow to process murine GP cartilage and adjacent bone to preserve resident cell ultrastructure, ECM proteins, and the composition and crystallinity of the mineral. To do this, we have compared the ultrastructure of GP prepared by different methods to determine the optimized preparation workflow for the GP.

This protocol has enabled direct observations linking intracellular CaP deposits with the extracellular mineralization processes including the involvement of intra- and extra-cellular vesicles in delivering transient CaP phases to promote collagen mineralization in the epiphyseal GP, during the early stages of postnatal, skeletal development.

2. Materials and methods

2.1. Sample preparation for TEM

Long bones (femur and tibia) were collected from 2- and 7- day-old CD1 and C57BL/6 mice immediately after sacrifice. The mice were maintained in accordance with the Home Office code of practice (for the housing and care of animals bred, supplied or used for scientific purposes). Day 2 and day 7 time points were selected to explore potential differences in cell-mediated mineralization in primary (which occurs at embryonic day16, E16) and secondary (which occurs by day 7 postnatal) centres of ossification. Long bones from CD1 wild-type mice were utilized in the sample preparation optimization studies, whereas long bones from C57BL/6 mice were employed in the mineralization study. It is important to note that ECM mineralization is a conserved process among vertebrates, and there are unlikely to be no discernible differences observed between these two mouse strains.

Samples were divided into 3 groups to examine the effectiveness of aqueous fixation and/or HPF to preserve cell and ECM ultrastructure and the composition and crystallinity of the mineral (Fig. 1).

Aqueous fixation prior to HPF. Dissected bones were fixed in Karnovsky solution (2 % formaldehyde and 2.5 % glutaraldehyde in 0.1 M PIPES) for 30 mins prior to vibratome sectioning. Sections were subjected to HPF and FS in acetone containing 1 % osmium tetroxide, 0.5 % uranyl acetate (UA), and 6 % water. Samples were held at −90 °C for 48 hrs, warmed up to −45 °C at the rate of 3.5 °C/hr, and held for 5 hrs, before warming to 0 °C. The samples were washed with cold acetone and progressively infiltrated by Epon 812 (Electron microscopy Sciences, Hatfield, PA, USA) at room temperature, and finally cured at 60 °C.

HPF without aqueous pre-fixation. Dissected bones were vibratome sectioned and subjected to HPF within 30 min of mouse sacrifice. The samples were then substituted in FS medium containing 0.5 % UA in acetone. The amount of water varied from completely anhydrous, to 1 %, and 6 % to understand the influence of water on tissue structure. The samples were held at –90 °C for 48 hrs and brought to −45 °C at 3.5 °C/hr. The samples were held again at −45 °C for 5 hrs, all washing was carried out at −45 °C. The samples were infiltrated in Low acryl HM20 resin (Agar Scientific, Essex, UK) while bringing the temperature up to −25 °C and cured under UV light at −25 °C for 48 hrs.

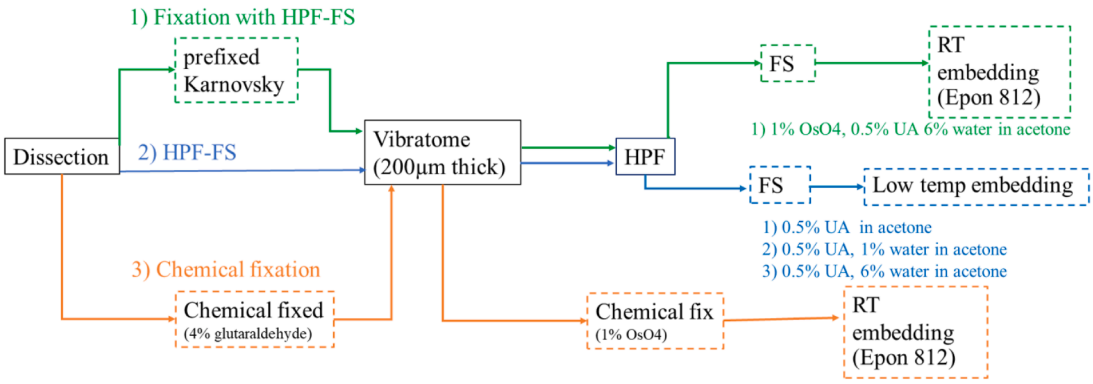

Fig. 1. Summary of the sample processing routes used to prepare the growth plate cartilage for transmission electron microscopy. The three different methods compared were 1) pre-chemical fixation followed by HPF-FS, 2) HPF-FS with varied % water and 3) chemical fixation.

Aqueous fixation only. Dissected bones were cut into half longitudinally and fixed in Karnovsky solution in 0.1 M PIPES buffer for 4 hrs at 4 °C and post-fixed in 1 % osmium tetroxide in 0.1 M PIPES buffer at room temperature for 1 hr, and dehydrated in a graded ethanol series from 50 %, 70 %, 90 %, and absolute ethanol. The tissues were progressively infiltrated with Epon 812 resin and polymerized at 60 °C.

2.2. Vibratome sectioning and high-pressure freezing

The bones were longitudinally sectioned to 180 μm using a Vibratome (Leica VT1200). For those destined for HPF, sections containing GP cartilage and adjacent metaphyseal bone were placed onto 6 mm planchets coated with hexadecane. The planchets were filled with 20 % dextran in 0.1 M Piperazine-N,N'-bis(2-ethanesulfonic acid). The sections were HPF at 2100 bar (Leica EM ICE).

2.3. Sectioning and microscopy

Resin-embedded tissues were sectioned to a thickness of 70 nm using an ultramicrotome (Leica EM UC7). The sections were collected on formvar coated slots and 3 mm copper grids without post-staining for TEM imaging and analysis. Bright-field TEM images were acquired on a JEOL 1400, operated at 80kV. Selected area electron diffraction (SAED), scanning transmission electron microscopy (STEM) (STEM) and electron dispersive x-ray spectroscopy (EDS) were performed on a JEOL 2100F200, operated at 200 kV. The samples were obtained from 2 mice per age group. High-angle annular dark field (HAADF)- STEM and EDS were performed on JEOL ARM200CF, operating at 200 kV.

3. Results

3.1. Optimization of a sample preparation protocol

We first compared the quality of preservation between GP cartilage prepared by conventional chemical fixation or HPF-FS with and without prior chemical fixation and with the inclusion of 0, 1, or 6 % water content. The pre-fixed HPF-FS sections exhibited a loss of membrane visibility (Fig.2a–c), while other structures including the nucleus, intracellular proteins, and collagenous matrix and macromolecules were well stained for contrast (Fig 2a–c). In Fig 2, the nucleus, and ribosomes on the endoplasmic reticulum were visible, but the lipid membranes that constituted the organelles were not visible. The empty spheres in Fig 2b and c (arrows) are probably mitochondria with no visible inner and outer membranes. Stained collagen fibrils were observed adjacent to the cellular region and calcified ECM was present in the vicinity (Fig 2c). However, intracellular mineral was rarely observed (Fig. 2b, dash arrows).

In GP cartilage that had been HPF (without pre-fixation) and FS in medium that contained 0 % (anhydrous), 1 % or 6 % water, the intracellular organelles (including the nucleus, Golgi body, endoplasmic reticulum and mitochondria), and ECM were well preserved with no evidence of ice crystal damage (Fig. 2e, i and m). The cartilage matrix proteins of the growth plate were well preserved and displayed no notable differences between the HPF sample prepared with varying amounts of water in the FS protocol (Fig. 2f, j, k and n). The tissue prepared using the anhydrous FS medium had sufficient contrast for observation, with lipid membranes and matrix proteins/macromolecules clearly visible. The addition of water, either 1 % or 6 % in the FS medium, demonstrated comparable contrast of membranes, cell organelles, and the ECM (Fig. 2e–p).

Electron-dense granules were observed intracellularly inside some mitochondria (Fig. 2g, j, k and o) and at higher magnification, the granular structure was not observed in prefixed-HPS samples (Fig. 2b and c). All preparations exhibited similar extracellular mineral clusters within the cartilage matrix which was comprised of needle-shaped minerals Fig.2d, h, l and p).

The ultrastructure of the GP prepared by conventional room temperature chemical fixation was not fully preserved (Fig.3). Some regions, particularly mineralized regions, were poorly infiltrated, resulting in ripped holes from sectioning. The chondrocytes appeared shrunken and densely stained which was also found in previous studies [34].

All images shown are from 2-day-old mice but the cellular morphology and localization of electron-dense granules within mitochondria were similar in the various preparations of the older 7-day-old mice.

3.2. Chondrocyte-regulated mineralization

We next investigated, in detail, the early mineralization stages of the endochondral ossification process using the anhydrous HPF-FS protocol as described in the previous section. This protocol provided sufficient membrane and organelle contrast and avoided the risk of any alterations of minerals in terms of both artifactual crystallinity [20] and mineral-granule dissolution. Mice aged 2 days and 7 days postnatal were selected for this study, representing active stages of mineralized tissue formation.

Longitudinal sections of long bone from 2- and 7-days old mice are shown in supplementary Fig.1. The ultrastructure of cells and matrix for both GP and bone are preserved and stained as described in Section 1. Bright-field TEM images demonstrated columns of proliferative chondrocytes and the mineralization of the ECM associated with hypertrophic chondrocytes (supplementary Fig.1a). By day 7, the secondary ossification center had developed in the epiphysis (supplementary Fig.1b). Fig.4a and b show chondrocytes in GP cartilage of 2-day old mice. Chondrocytes in the proliferative and hypertrophic zones

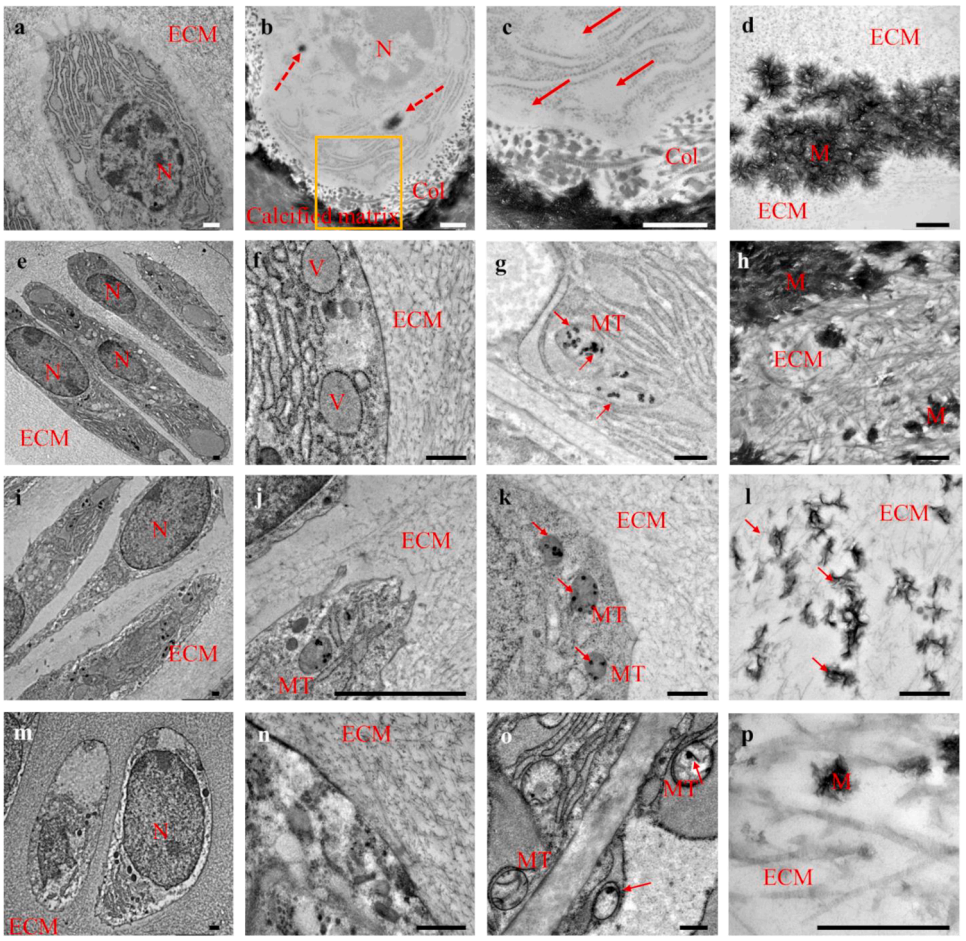

Fig. 2. a–d) Bright-field TEM images taken from day 2 postnatal mouse tissue showing chondrocytes in dissected growth plate cartilage prepared by prefixation using the Karnovsky protocol, and HPF-FS using a 1 % osmium tetroxide, 0.5 % uranyl acetate and 6 % water in acetone solution. a) Chondrocytes within the cartilage matrix, b) Chondrocyte containing intracellular mineral (dash arrows) adjacent to the calcified matrix, c) High magnification image of (b; box) showing that the plasma membrane exhibits a very faint contrast and very poor structural preservation of the mitochondria (arrows) and ER membranes (arrows). d) Cluster of needle shape mineral deposits in extracellular matrix. Scale bar = 500 nm. e–h) Bright-field TEM images taken from day 2 postnatal mouse tissue showing the ultrastructure of growth plate cartilage prepared by HPF- FS using anhydrous acetone with 0.5 % uranyl acetate. e) Chondrocyte embedded in the cartilage matrix, f) Part of a chondrocyte (left) with its intracellular vesicles (V) organelles and clear structural definition of the plasma membrane adjacent to cartilage matrix (right) showing fine structure of collagenous network, g) Mitochondria containing electron-dense granules (arrows) next to the endoplasmic reticulum, h) Mineral deposits in the extracellular matrix. Scale bar = 500 nm. i–l) Bright-field TEM images taken from day 2 postnatal mouse tissue showing the ultrastructure of growth plate cartilage prepared by HPF-FS in anhydrous acetone with 0.5 % uranyl acetate and 1 % water. i) Array of chondrocytes embedded cartilage matrix, j and k) Part of a chondrocyte (left) with its intracellular cellular organelles and mitochondria containing electron-dense granules (arrows), adjacent to the collagenous cartilage matrix. l) Needle-shaped mineral deposits in the cartilage matrix. Scale bar = 500 nm. m–p) Bright-field TEM images taken from day 2 postnatal mouse tissue showing the ultrastructure of growth plate cartilage prepared by HPF- FS in anhydrous acetone with 0.5 % uranyl acetate and 6 % water. m) Chondrocytes in the growth plate cartilage, n) Part of a chondrocyte showing intracellular organelles (left) and adjacent cartilage matrix (right; ECM), o) Mitochondria in chondrocytes (left and right) containing electron-dense granules (arrows), p) Clusters of needle shape mineral (M) in the cartilage matrix (ECM). *N*= nucleus, ECM= extracellular matrix, MT=mitochondria, *V*=vesicle, *M*= mineral deposits. Scale bar = 500 nm.

contained electron-dense granules within mitochondria (Fig 4a and b, arrows) and in intracellular vesicles with a diameter of 0.5–1 μm (Fig. 4d). Similar sized vesicles containing several granules were observed within the ECM adjacent to the chondrocytes (Fig.4c, arrows), while a lower contrast vesicle adjacent to collagen fibrils contained only individual electron-dense granules (Fig. 4c, box). These nanosized globular granules were also observed on collagen fibrils together with needle-shaped crystals (Fig. 4e, arrows). Chondrocytes in the calcified hypertrophic zone also contained these intracellular electron-dense granules (Fig. 4f). Chemical analysis by EDS confirmed the presence of Ca and P in the intracellular and collagen fibril-associated electron-dense granules (Fig.5a–c). Hollow, ring-like structures were frequently observed by HAADF-STEM in the region between the chondrocytes and the ECM (Fig. 5d). EDS maps confirmed these structures were composed of calcium and phosphorus (Fig.5d and supplementary Fig. 2), indicating a calcified "crust" of material encasing these ring-like structures.

By day 7, intracellular mineral granules were also seen within chondrocytes but in addition to these, smaller empty vesicles (100–200 nm in diameter) budding from the plasma membrane of the chondrocytes were noted (Fig. 6a–c). Furthermore, we observed similar sized globular clusters of needle-like mineral crystals in the chondrocyte ECM (Fig.7) and also associated with the collagen matrix in the calcified zone (Fig. 6d). These were observed in both day 2 and 7 samples. These structures had a similar size, which matched the size of MVs [4,35] and were filled with Ca and P (Supplementary Fig. 3). SAED from minerals within these MVs displayed a weak diffuse ring pattern, which indicates that the mineral has a short to medium-range order (Fig. 7). The mineral crystals were needle-shaped and mineral *foci* were associated with the type II collagen-rich matrix of cartilage (Fig 8a and b) whereas in the

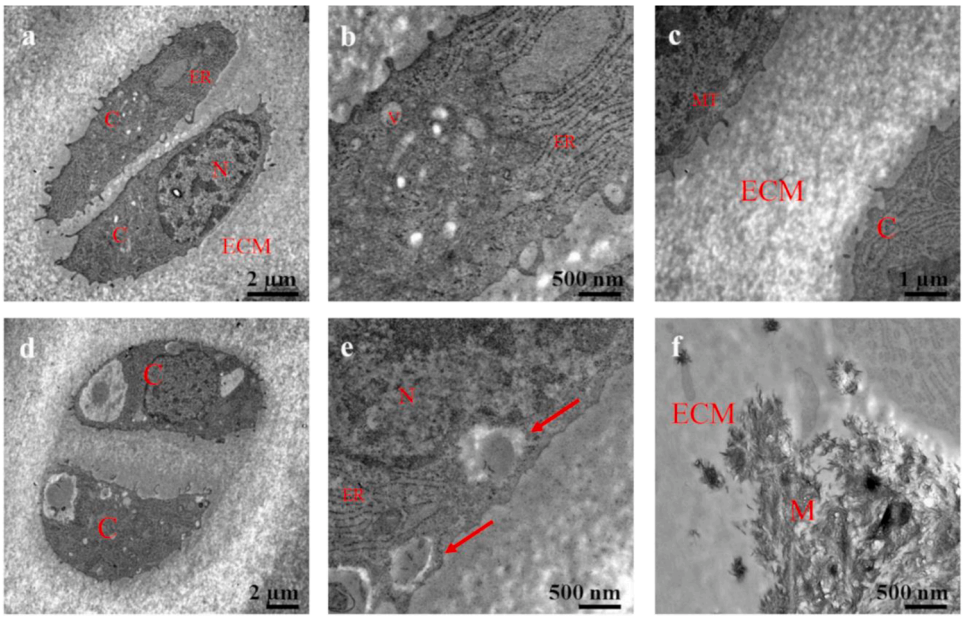

Fig. 3. Bright-field TEM images taken from day 2 postnatal mouse tissue showing the ultrastructure of chemically fixed growth plate. a) Chondrocytes in the extracellular matrix, b) Cellular organelles, c) Cartilage matrix, d) Chondrocytes in lacunae, e) Shrunken and damaged mitochondria (arrows) inside a chondrocyte, f) Mineralized matrix. C-chondrocyte, N-nucleus, endoplasmic reticulum -ER, mitochondria - MT, ECM- extracellular matrix, M - mineral deposit.

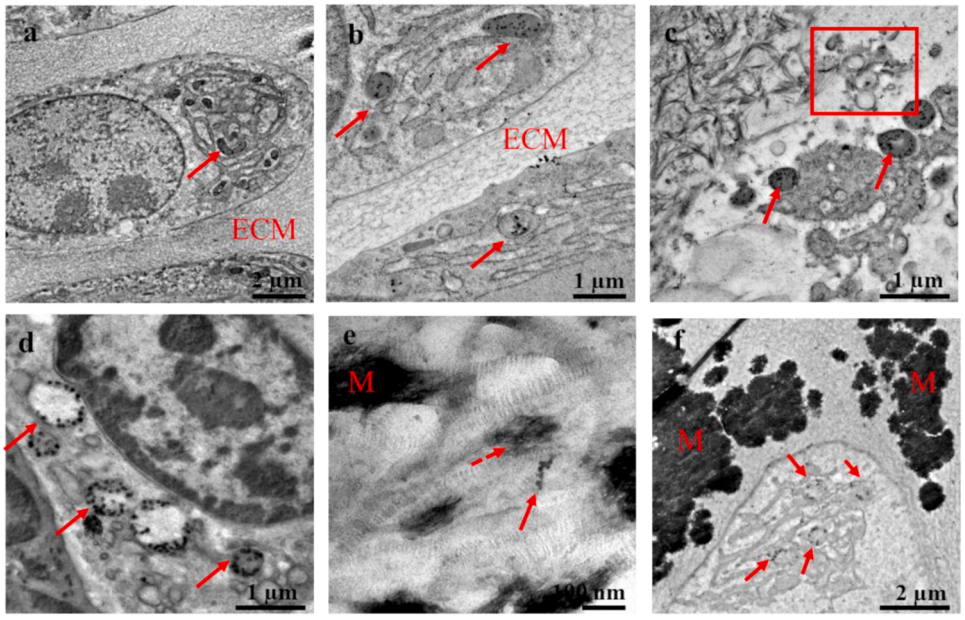

Fig. 4. Bright-field TEM images taken from day 2 postnatal mouse tissue showing a) Chondrocytes in cartilage matrix (ECM) containing mitochondria with electron-dense granules (arrows), b) Electron dense granules in mitochondria (arrows) near ER, c) Extracellular vesicle containing electron dense granules (arrows), and top right; vesicle with a granule inside next to another 2 empty vesicles nearby (box), d) Electron-dense granules inside intracellular vesicles (arrows) with 2 different matrix densities, e) Electron-dense granules on collagen fibrils (arrows) among deposits of mineral crystals (dashed arrows), f) Larger calcified cartilage matrix (M) adjacent to the chondrocyte that contains intracellular granules (arrows).

metaphyseal bone the mineral crystals were aligned along the collagen type 1 fibrils (Fig 8c and d). In addition, we observed a sac-like structure among clusters of needle-shaped minerals in STEM mode (Fig. 9, arrows). This structure was filled with PO (Fig. 9a), which suggests that it may be composed of a lipid membrane. Additionally, the results from both Day 2 and Day 7 indicate that chondrocytes contribute to cartilage mineralization using similar organelles at both time points.

4. Discussion

This lack of clarity on the process by which collagen fibrils mineralize is a consequence of sample preparation protocols that have not been optimized to simultaneously preserve both mineral composition/crystallinity and tissue structure. Prior reports are also vague about whether they introduce water into the tissues during sample fixation and processing. Water is introduced to assist with fixation and contrast staining of cell organelles/collagen fibrils for TEM, but it will

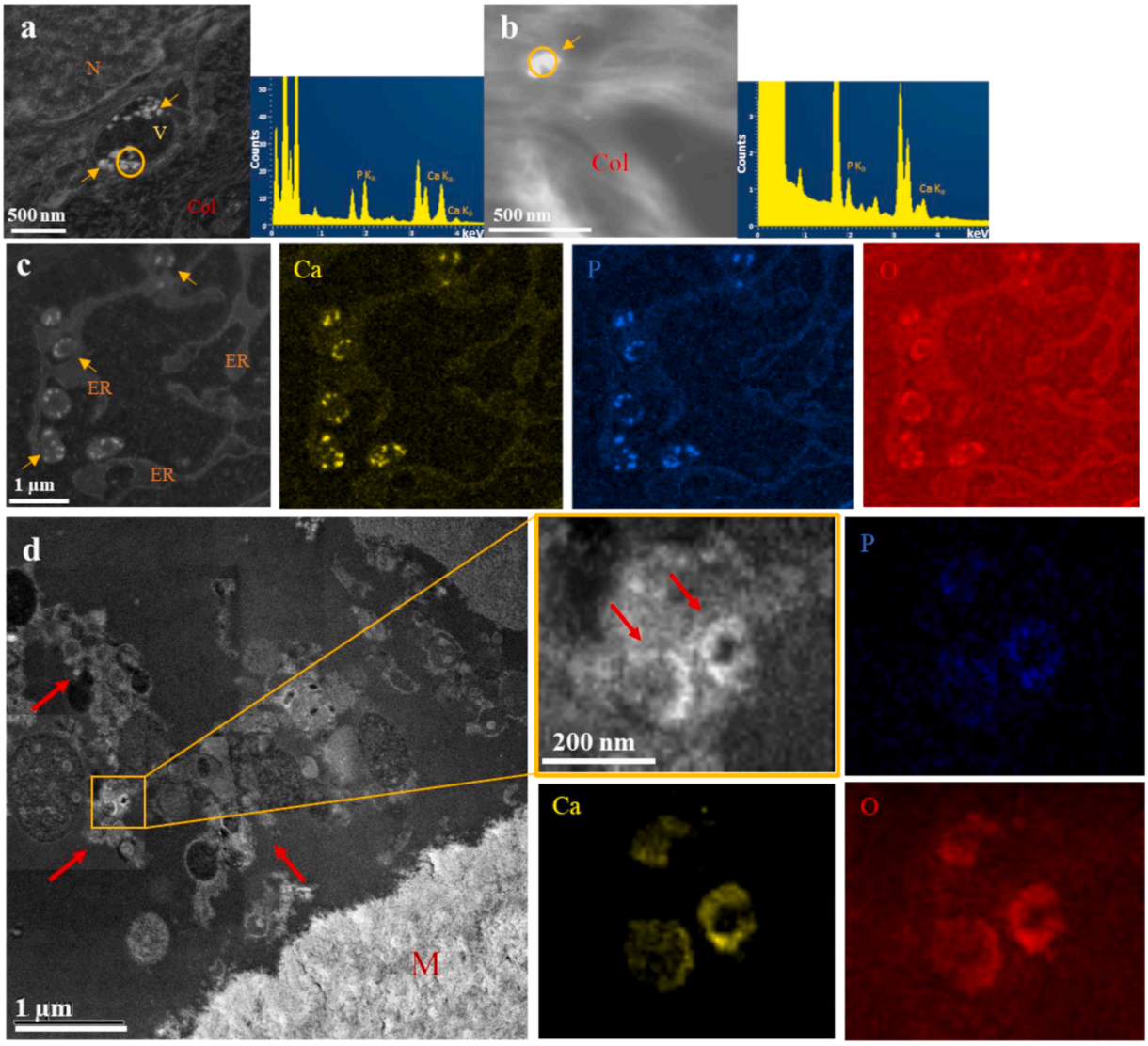

Fig. 5. Dark-field STEM images and EDS compositional mapping taken from day 2 postnatal mice tissue showing a) Intracellular vesicle that contain electron-dense granules (arrows), b) electron-dense granule on collagen fibrils (arrow). *N* = nucleus, *V*= intracellular vesicle, Col = collagen fibrils. EDS spectra taken from the marked granules show Ca and P in both intracellular and extracellular granules. c) Dark-field STEM image of mitochondria in a chondrocyte that contains electron dense granules (arrows) and elemental mapping confirming a presence of Ca, P and O in those granules. d) Dark-field STEM image of extracellular rings (arrows) of minerals outside the chondrocytes and near the mineralized region (M), and P, Ca, and O elemental maps of the boxed area.

redistribute the mineral/ions and change their structure and crystallinity making the results liable to misinterpretation [20]. Fixing samples before HPF is often employed to reduce morphological artifacts due to necrosis of samples that require a long dissection period. Our results indicated that the GP which was prefixed before HPF-FS lost membrane visibility, and the addition of water in the FS medium did not recover the contrast (Fig.2). One previous study showed the ultrastructure of cells with reverse contrast of nuclear and mitochondria membranes of human skin. The skin was prepared by fixing in 2.5 % glutaraldehyde at 4 °C overnight before rapid freezing and FS in acetone with 2 % osmium tetroxide, followed by room temperature embedding [36]. Conversely, other studies demonstrated preserved and visible membrane structures. As an example, a wool follicle was prefixed before HPF-FS (in acetone with 2 % osmium tetroxide, 1 % glutaraldehyde, and 10 % of water), resulting in a good membrane contrast [26]. The majority of previous studies focused on cryo-fixation of cultured cells, and therefore the pre-fixing step prior to freezing was not required. The cause of chondrocyte membrane contrast loss in prefixed GP remains inconclusive, *i.e.* whether it is attributed solely to prefixation, or if it is in combination with other parameters.

All the GP prepared by HPF-FS without prefixation step were well preserved; there were no signs of artifacts of ultrastructure nor shrinkage of chondrocytes. All the cartilage matrices appeared as a fine network of collagen, with no difference in terms of preservation of cell ultrastructure in the samples prepared with variable amounts of water (0, 1 or 6 %). The addition of water into FS has been suggested to enhance staining contrast of organic materials. Previous work demonstrated that the addition of 5 % water improved membrane contrast of yeast cells when compared to water-free FS medium [31]. In pancreatic tissue, 1 % water in acetone containing osmium tetroxide was sufficient to enhance membrane visibility compared to the anhydrous FS condition [31].

In chemical fixed samples, the cartilage matrix which comprises type II collagen, proteoglycan, and macromolecules lacked a distinct structure (Fig.3). This is similar to a previous study showing that chemical fixation by an aldehyde-based medium led to a distortion of the macromolecules [22]. It is also difficult to avoid artifacts during dehydration and the subsequent embedding steps. For example, the use of an initial 40 % ethanol for dehydration causes cartilage swelling, although this

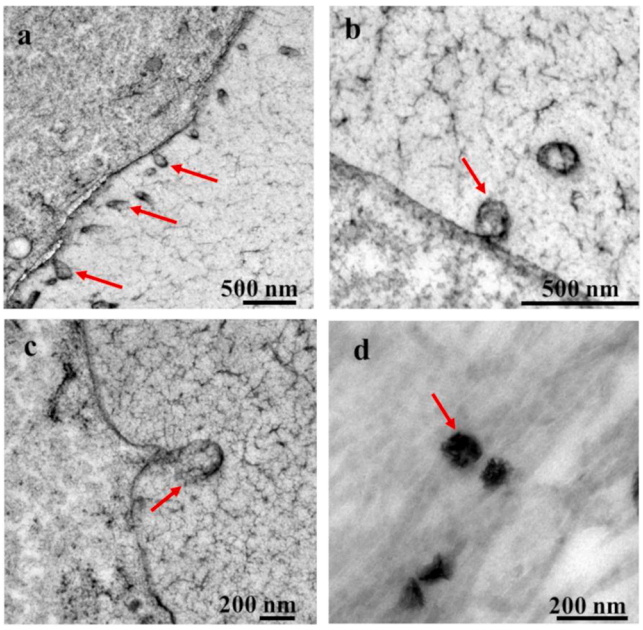

Fig. 6. Bright field TEM images of day 7 postnatal mouse tissue showing (a) Vesicles 100 nm in diameter budding from the plasma membrane of chondrocytes (arrows), b and c) Higher magnification images of 100 nm diameter extracellular vesicles budding from chondrocyte membrane, d) Globular mineral cluster with a size of 100 nm associated with collagen fibrils.

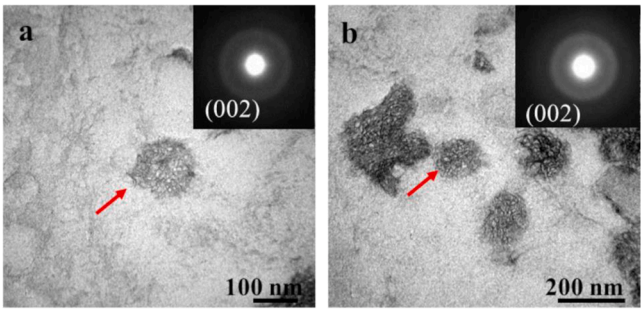

Fig. 7. a and b) Confined globular minerals with size ranges between 100 and 150 nm in ECM, insets are diffraction patterns obtained from marked areas (arrow) in a and b, taken from the samples of day 2 postnatal mice.

might be avoided by an initial dehydration in 70 % ethanol [21]. If the cartilage is mechanically compressed during its excision, reswelling cannot be avoided even with initial dehydration in 100 % ethanol [37]. In summary, the GP prepared by HPF without a pre-fixation step and anhydrous FS medium-acetone with 0.5 % UA is well preserved. The omission of water did not yield any adverse effect on contrast staining.

The literature on cartilage matrix mineralization has not advanced significantly since the initial observations by Anderson and Bonucci in the late 1960s where they proposed that MVs bud of from the chondrocyte plasma membrane and sequester mineral. Our study of mineralization in GP cartilage/bone demonstrated the presence of two pathways that potentially contributed to cartilage mineralization by chondrocytes: i) intracellular-originating and ii) extracellular-originating pathways. *For the intracellular originating pathway*, CaP granules were observed inside mitochondria and intracellular vesicles within proliferative and hypertrophic chondrocytes. The occurrence of CaP granules inside the mitochondria has been reported in previous mineralization studies [14,18,38]. These intramitochondrial granules are believed to form as an ACP complex [39]. Several studies have shown that both endoplasmic reticulum and mitochondria of

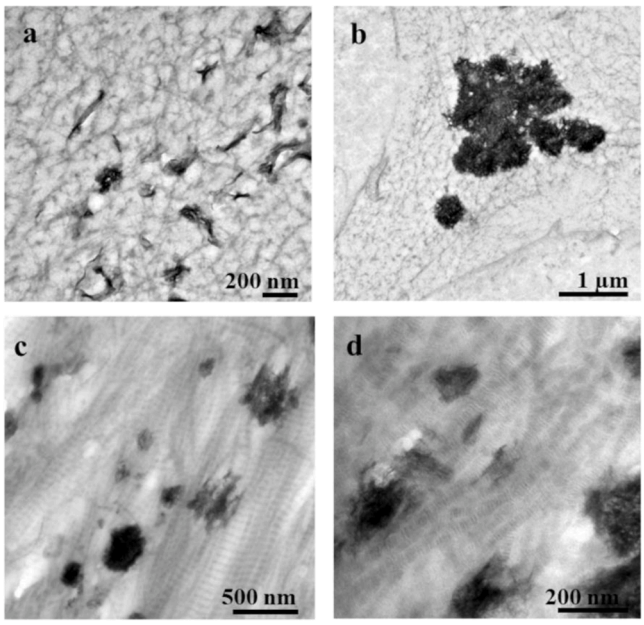

Fig. 8. Bright field TEM images showing mineral deposits in the ECM of cartilage and adjacent bone taken from day 7 postnatal mice tissue. a - b) Mineral associated with type II collagen and proteoglycan network in growth plate cartilage. c - d) Mineral associated with type I collagen in bone.

mineralizing cells contained elevated levels of calcium ions [40,41]. The origin of intra-mitochondrial CaP is proposed to originate from endoplasmic reticulum and be transported in the form of either ion or CaP clusters to the mitochondria [16]. This was demonstrated by HAADF - STEM combined with EDS of embryonic parietal bone of C57BL/6 mice [16]. Another study employing live cell imaging with fluorescent staining demonstrated a co-localization of lysozyme with intracellular CaP vesicles in KUSA-A1 mouse osteoblastic cells [38]. Others have proposed that the CaP-containing intracellular vesicles found in human dental pulp stem cells are autophagosomes [18]. CaP granules inside mitochondria may be transported to intracellular vesicles by a process of mitophagy (autophagy of mitochondria), in which damaged mitochondria are engulfed by phagosomes, later fusing with lysosomes and eventually extracellularly transported via exocytosis [18]. This is believed to be part of a cell-regulated mineralization process as inhibition of mitophagy has been shown to result in a reduction of osteogenesis [18], and treatment of KUSSA-A1 osteoblast cells by endosidin 2 (lysosomal exocytosis inhibitor) or vacuolin-1 (exocytosis inhibitor) resulted in intracellular accumulation of CaP with little or no exocytosis [38].

Here we present supporting evidence suggesting that CaP granules are transported from cells to the ECM in intact vesicles; possibly phagosomes (Fig. 4c). The intracellular-originating vesicles with a size of approximately 0.5–1 μm are relatively large when compared to the MVs. These intracellular-originating vesicles are filled with spherical CaP granules, which are later transferred to collagen fibrils in the ECM (Fig. 4b). This evidence could suggest that these 0.5–1 μm vesicles which originated intracellularly may act as a carrier to transport CaP granules from the mitochondria to the collagen matrix. However, how these nanogranules are released from the intracellular-originating vesicles to collagen fibrils remains unclear. The images shown in Fig.4c and e might suggest how they transport from the vesicles, and transfer to the collagen matrix. However, TEM-based techniques provide only snapshots of various stages of the mineralization process. Consequently, these images represent isolated events, rather than a continuous sequence of biological events. As a result, there is no dynamic understanding of the mechanisms underlying biomineralization.

In addition, we also observed the budding of vesicles (with a size of

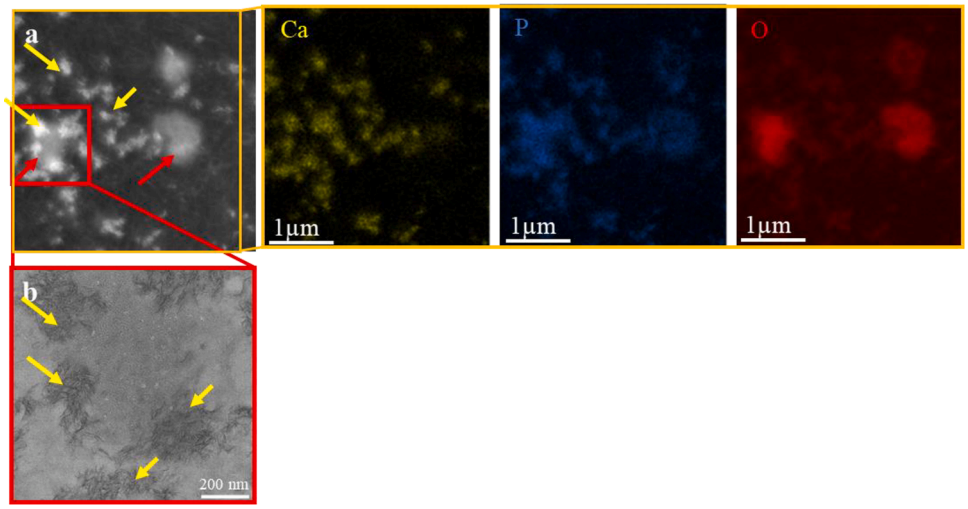

Fig. 9. a) Dark-field STEM image taken from day 2 postnatal mouse GP and corresponding Ca, P and O EDS elemental maps of the region marked in the orange box showing the colocation of Ca, P, and O on the collagen matrix. Clusters of needle-shaped dense material (yellow arrows) contain both Ca and P, while more diffuse vesicle-like structures (red arrows) contain P and O. b) Higher magnification bright-field TEM image of the boxed region in a, showing clusters of needle shape mineral clusters (yellow arrows) within the vesicle-like structure.

100–200 nm) from the plasma membrane of GP chondrocytes which resemble the MV first described in the 1960s [42,43]. The subsequent mineralization of these MVs may be through the activities of phosphatases and annexins as previously suggested [6]. The vesicle membrane may rupture (Fig. 9) and release the mineral crystals into the extracellular space and onto the collagen fibrils, as observed as globular mineral *foci* on collagen fibrils (Figs. 6d, 7a-b, 8b-c, and supplementary fig. 3). Notably, we also observed hollow, ring-like CaP structures outside the chondrocytes and near the mineralized region (Fig. 5d). To our knowledge these structures have not been observed previously but could be a snapshot of extracellular vesicles off-loading their mineral cargo. Both cell-regulated mechanisms reported in this study involve sequestering CaP inside membrane-bound vesicles. The vesicles, however have different origins, sizes, and mechanisms by which they acquire CaP and contain different types of mineral morphology and crystallinity. These observations support a theory that there are two routes by which chondrocytes mineralize their surrounding matrix in epiphyseal cartilage at the growth plate and provide fresh insight into the endochondral ossification process.

It has long been recognised that the vertically orientated longitudinal septa, and not the transverse septa, of the growth plate are mineralised [3]. Accordingly, MVs have been shown to arise by budding off from the lateral surfaces of the chondrocytes juxtaposed to the longitudinal septal matrix [3,44,45]'. This intimate association of MVs with the longitudinal septa suggests an element of polarity in the secretion MVs from the chondrocyte and therefore this must also be the case for intracellular vesicles if they also contribute to the mineralisation of the longitudinal septal matrix. It is noteworthy that similar polarity also exists in osteoblasts where MVs arise from the basal plasma membrane adjacent to the newly formed osteoid [46].

5. Conclusions

Here, we present evidence of how chondrocytes contribute to bone mineralization using TEM and STEM by using appropriate sample preparation techniques. Two parallel mineralization processes driven by chondrocytes were observed including: 1) intracellular- and 2) extracellular-originating mineralized vesicles. This intracellular route for the delivery of CaP mineral has not been previously recognized in epiphyseal cartilage but its identification here suggests a novel mineralisation process that is in addition to MVs which are believed to form by an ectosomal/microvesicles budding mechanism. This knowledge of an alternative intracellular mineralisation route now needs to be extended to fully understand how the mineral is trafficked from the mitochondria to the vesicles and out into the ECM. Furthermore, the requirement for phosphatases such as TNAP and PHOSPHO1, widely recognized to be essential for bone and cartilage mineralisation, for the formation of the intracellular mineral are unclear and requires further investigation.

Here we developed a new cryofixation preparation route for TEM imaging that has disclosed a cell-regulated process of mineralization in epiphyseal cartilage. The notable advantage of the HPF-FS techniques was its ability to preserve tissue in a near-native state in combination with plastic embedding. This makes the sample tolerant to the electron dose, enabling application of analytical techniques downstream in the workflow. High resolution TEM images revealed an involvement of mitochondria and intracellular and extracellular vesicles in delivering transient mineral phases to the collagen fibrils to promote cartilage mineralization in developing epiphyseal cartilage. The protocols developed will benefit skeletal research, providing an improved understanding of bone mineralization. The techniques could be adapted in to understanding of the cell based origins of pathological mineralization in soft tissues such as cardiovascular, ocular, brain, and smooth muscle. For example, they could be adapted to determine if the transdifferentiation of vascular smooth muscles into an osteogenic phenotype during vascular calcification is associated with both the intracellular and extracellular mineralisation routes. A better understanding of the skeletal cellular mineralisation mechanisms should also guide tissue engineering approaches for restoring bone or pharmaceutical interventions for encouraging bone formation.

CRediT authorship contribution statement

Suwimon Boonrungsiman: Writing – review & editing, Writing – original draft, Visualization, Validation, Methodology, Investigation, Funding acquisition, Formal analysis, Data curation, Conceptualization. **Christopher Allen:** Investigation, Data curation. **Fabio Nudelman:** Writing – review & editing, Supervision. **Sandra Shefelbine:** Writing – review & editing, Supervision. **Colin Farquharson:** Writing – review & editing, Supervision. **Alexandra E Porter:** Writing – review & editing, Supervision, Methodology, Conceptualization. **Roland A Fleck:** Writing – review & editing, Supervision, Methodology, Funding acquisition, Conceptualization.

Declaration of competing interest

The authors declare that they have no known competing financial interests or personal relationships that could have appeared to influence the work reported in this paper.

Acknowledgments

This project has received funding from the European Union's Horizon 2020 research and innovation program under the Marie Skłodowska-Curie grant agreement No 893404. CF acknowledges financial support from the Biotechnology and Biological Sciences Research Council (BBSRC) in the form of an Institute Strategic Program Grant (BBS/E/D/10002071 and BBS/E/RL/230001C). For the purpose of open access, the authors have applied a CC-BY public copyright license to any Author Accepted Manuscript version arising from this submission.

Supplementary materials

Supplementary material associated with this article can be found, in the online version, at doi:10.1016/j.actbio.2024.11.015.

References

[1] H.M. Kronenberg, Developmental regulation of the growth plate, Nature 423 (6937) (2003) 332–336.
[2] E.B. Hunziker, Mechanism of longitudinal bone growth and its regulation by growth plate chondrocytes, Microsc. Res. Tech. 28 (6) (1994) 505–519.
[3] H.C. Anderson, Electron microscopic studies of induced cartilage development and calcification, J. Cell Biol. 35 (1) (1967) 81–101.
[4] H.C. Anderson, Matrix vesicles and calcification, Curr. Rheumatol. Rep. 5 (3) (2003) 222–226.
[5] L. Hessle, K.A. Johnson, H.C. Anderson, S. Narisawa, A. Sali, J.W. Goding, R. Terkeltaub, J.L. Millan, Tissue-nonspecific alkaline phosphatase and plasma cell membrane glycoprotein-1 are central antagonistic regulators of bone mineralization, Proc. Natl. Acad. Sci. U.S.A. 99 (14) (2002) 9445–9449.
[6] J.L. Millán, The role of phosphatases in the initiation of skeletal mineralization, Calcif. Tissue Int. 93 (4) (2013) 299–306.
[7] S. Dillon, K.A. Staines, J.L. Millán, C. Farquharson, How to build a bone: PHOSPHO1, biomineralization, and beyond, JBMR Plus 3 (7) (2019) e10202.
[8] L. Cui, D.A. Houston, C. Farquharson, V.E. MacRae, Characterization of matrix vesicles in skeletal and soft tissue mineralization, Bone 87 (2016) 147–158.
[9] T. Kirsch, G. Harrison, E.E. Golub, H.D. Nah, The roles of annexins and types II and X collagen in matrix vesicle-mediated mineralization of growth plate cartilage, J. Biol. Chem. 275 (45) (2000) 35577–35583.
[10] M. Yamada, Ultrastructural and cytochemical studies on the calcification of the tendon-bone joint, Arch. Histol. Jpn. 39 (5) (1976) 347–378.
[11] W. Wu, H. Zhuang, G.H. Nancollas, Heterogeneous nucleation of calcium phosphates on solid surfaces in aqueous solution, J. *Biomed. Mater. Res* 35 (1) (1997) 93–99.
[12] F. Nudelman, K. Pieterse, A. George, P.H.H. Bomans, H. Friedrich, L.J. Brylka, P.A. J. Hilbers, G. de With, N.A.J.M. Sommerdijk, The role of collagen in bone apatite formation in the presence of hydroxyapatite nucleation inhibitors, Nat. Mater. 9 (12) (2010) 1004–1009.
[13] W.J. Landis, M.J. Song, A. Leith, L. McEwen, B.F. McEwen, Mineral and organic matrix interaction in normally calcifying tendon visualized in three dimensions by high-voltage electron microscopic tomography and graphic image reconstruction, J. Struct. Biol. 110 (1) (1993) 39–54.
[14] S. Boonrungsiman, E. Gentleman, R. Carzaniga, N.D. Evans, D.W. McComb, A. E. Porter, M.M. Stevens, The role of intracellular calcium phosphate in osteoblast-mediated bone apatite formation, Proc. Natl. Acad. Sci. U.S.A. 109 (35) (2012) 14170–14175.
[15] J. Mahamid, B. Aichmayer, E. Shimoni, R. Ziblat, C. Li, S. Siegel, O. Paris, P. Fratzl, S. Weiner, L. Addadi, Mapping amorphous calcium phosphate transformation into crystalline mineral from the cell to the bone in zebrafish fin rays, Proc. Natl. Acad. Sci. U.S.A. 107 (14) (2010) 6316–6321.
[16] C. Tang, Y. Wei, L. Gu, Q. Zhang, M. Li, G. Yuan, Y. He, L. Huang, Y. Liu, Y. Zhang, Biomineral precursor formation is initiated by transporting calcium and phosphorus clusters from the endoplasmic reticulum to mitochondria, Adv. Sci. 7 (8) (2020) 1902536.
[17] J.O. Strubbe-Rivera, J.R. Schrad, E.V. Pavlov, J.F. Conway, K.N. Parent, J.N. Bazil, The mitochondrial permeability transition phenomenon elucidated by cryo-EM reveals the genuine impact of calcium overload on mitochondrial structure and function, Sci. Rep. 11 (1) (2021) 1037.
[18] D.-d. Pei, J.-l. Sun, C.-h. Zhu, F.-c. Tian, K. Jiao, M.R. Anderson, C. Yiu, C. Huang, C.-x. Jin, B.E. Bergeron, J.-h. Chen, F.R. Tay, L.-n. Niu, Contribution of mitophagy to cell-mediated mineralization: revisiting a 50-year-old conundrum, Adv. Sci. 5 (10) (2018) 1800873.
[19] E.D. Eanes, Amorphous calcium phosphate: thermodynamic and kinetic considerations, in: Z. Amjad (Ed.), Calcium Phosphates in Biological and Industrial Systems, Springer US, Boston, MA, 1998, pp. 21–39.
[20] C. Combes, C. Rey, Amorphous calcium phosphates: synthesis, properties and uses in biomaterials, Acta Biomater. 6 (9) (2010) 3362–3378.
[21] E.B. Hunziker, R.K. Schenk, Physiological mechanisms adopted by chondrocytes in regulating longitudinal bone growth in rats, J. Physiol. 414 (1989) 55–71.
[22] E.B. Hunziker, R.K. Schenk, Cartilage ultrastructure after high pressure freezing, freeze substitution, and low temperature embedding. II. Intercellular matrix ultrastructure - preservation of proteoglycans in their native state, J. Cell Biol. 98 (1) (1984) 277–282.
[23] J.D. Szafranski, A.J. Grodzinsky, E. Burger, V. Gaschen, H.H. Hung, E.B. Hunziker, Chondrocyte mechanotransduction: effects of compression on deformation of intracellular organelles and relevance to cellular biosynthesis, Osteoarthr. Cartil. 12 (12) (2004) 937–946.
[24] G.E. Sosinsky, J. Crum, Y.Z. Jones, J. Lanman, B. Smarr, M. Terada, M.E. Martone, T.J. Deerinck, J.E. Johnson, M.H. Ellisman, The combination of chemical fixation procedures with high pressure freezing and freeze substitution preserves highly labile tissue ultrastructure for electron tomography applications, J. Struct. Biol. 161 (3) (2008) 359–371.
[25] E. Shimoni, M. Müller, On optimizing high-pressure freezing: from heat transfer theory to a new microbiopsy device, J. Microsc. 192 (Pt 3) (1998) 236–247.
[26] S. Velamoor, M. Richena, A. Mtrchell, S. Lequeux, M. Bostina, D. Harland, High-pressure freezing followed by freeze substitution of a complex and variable density miniorgan: the wool follicle, J. Microsc. 278 (1) (2020) 18–28.
[27] D.M.R. Harvey, Freeze-substitution, J. Microsc. 127 (2) (1982) 209–221.
[28] D. Studer, B.M. Humbel, M. Chiquet, Electron microscopy of high pressure frozen samples: bridging the gap between cellular ultrastructure and atomic resolution, Histochem. Cell Biol. 130 (5) (2008) 877–889.
[29] C. Buser, P. Walther, Freeze-substitution: the addition of water to polar solvents enhances the retention of structure and acts at temperatures around –60 °C, J. Microsc. 230 (2) (2008) 268–277.
[30] A.M. Glauert, P.R Lewis, In biological specimen preparation for transmission electron, Microsc. Microanal 6 (5) (1998) 478–479.
[31] P. Walther, A. Ziegler, Freeze substitution of high-pressure frozen samples: the visibility of biological membranes is improved when the substitution medium contains water, J. Microsc. 208 (1) (2002) 3–10.
[32] T. Akisaka, G.P. Subita, Y. Shigenaga, Ultrastructural observations on chick bone processed by quick-freezing and freeze-substitution, Cell Tissue Res. 247 (3) (1987) 469–475.
[33] L. Ameye, R. Hermann, P. Dubois, Ultrastructure of sea urchin calcified tissues after high-pressure freezing and freeze substitution, J. Struct. Biol. 131 (2) (2000) 116–125.
[34] E.B. Hunziker, K. Lippuner, N. Shintani, How best to preserve and reveal the structural intricacies of cartilaginous tissue, Matrix Biol. 39 (2014) 33–43.
[35] Y. Wei, C. Tang, J. Zhang, Z. Li, X. Zhang, R.J. Miron, Y. Zhang, Extracellular vesicles derived from the mid-to-late stage of osteoblast differentiation markedly enhance osteogenesis *in vitro* and *in vivo*, Biochem. Biophys. Res. Commun. 514 (1) (2019) 252–258.
[36] M. Yamaguchi, S. Wakabayashi, Y. Nakamura, H. Matsue, T. Hirao, S. Aoki, S. Yamashina, H. Yamada, N. Mamizu, H. Furukawa, H. Chibana, Good ultrastructural preservation of human tissues and cultured cells by glutaraldehyde fixation, sandwich freezing, and freeze-substitution, Cytologia (Tokyo) 85 (1) (2020) 15–26.
[37] J.M. Clark, Dimensional changes of articular cartilage during immersion freezing and freeze substitution for scanning electron microscopy, Scan. Microsc. 12 (3) (1998) 465–474.
[38] T. Iwayama, T. Okada, T. Ueda, K. Tomita, S. Matsumoto, M. Takedachi, S. Wakisaka, T. Noda, T. Ogura, T. Okano, P. Fratzl, T. Ogura, S. Murakami, Osteoblastic lysosome plays a central role in mineralization, Sci. Adv. 5 (7) (2019) eaax0672.
[39] A.S. Posner, F. Betts, N.C. Blumenthal, Properties of nucleating systems, Metab. Bone Dis. Relat. Res. 1 (2) (1978) 179–183.
[40] L. Daverkausen-Fischer, F. Pröls, Regulation of calcium homeostasis and flux between the endoplasmic reticulum and the cytosol, J. Biol. Chem. 298 (7) (2022) 102061.
[41] E. Carafoli, The regulation of intracellualr calcium, in: S.G. Massry, J.M. Letteri, E. Ritz (Eds.), Regulation of Phosphate and Mineral Metabolism, Springer US, Boston, MA, 1982, pp. 461–472.
[42] E. Bonucci, Fine structure of early cartilage calcification, J. Ultrastruct. Res. 20 (1) (1967) 33–50.
[43] R.N.A. Cecil, H. Clarke Anderson, Freeze-fracture studies of matrix vesicle calcification in epiphyseal growth plate, Metab. Bone Dis. Relat. Res. 1 (2) (1978) 89–95.
[44] F.P. Reinholt, A. Wernerson, Septal distribution and the relationship of matrix vesicle size to cartilage mineralization, Bone Miner. 4 (1) (1988) 63–71.
[45] D.R. Simon, I. Berman, D.S. Howell, Relationship of extracellular matrix vesicles to calcification in normal and healing rachitic epiphyseal cartilage, Anat. Rec. 176 (2) (1973) 167–179.
[46] D.C. Morris, K. Masuhara, K. Takaoka, K. Ono, H.C. Anderson, Immunolocalization of alkaline phosphatase in osteoblasts and matrix vesicles of human fetal bone, Bone Miner. 19 (1992) 287–298.